
3-2 Detector

3-2-1 Terahertz Frontside-Illuminated Quantum Well Photodetector

Mikhail Patrashin and HOSAKO Iwao

We have demonstrated the operation of a frontside-illuminated GaAs/AlGaAs quantum well photodetector based on intersubband absorption in a quantum well (QW) with a targeted peak frequency of 3 THz. A multiple quantum well structure consists of 20 periods of 18 nm QWs interleaved by 80 nm barriers with an Al alloy content of 2 %. We measured the following performance characteristics: dark current, responsivity, and spectral response. A responsivity of 13 mA/W at an electric bias of 40 mV and an operating temperature of 3 K was obtained with a peak response close to the designed detection frequency. The dark current density was a few $\mu\text{A}/\text{cm}^2$ and was limited by thermally assisted tunneling through the barriers. We looked also at possible designs to optimize the device's performance.

Keywords

Terahertz, Quantum well photodetector, Intersubband transition

There have been continuing efforts in recent years to develop practical sources and detectors of terahertz (THz) radiation[1]-[9]. Future applications of terahertz imaging, spectroscopy and communications will use direct and heterodyne detection techniques that require suitable THz sources and fast, sensitive multi-element detectors. There have traditionally been very limited choices of detectors in the terahertz region of the spectrum. Significant improvements have been achieved in the performance of mixers for heterodyne receivers below 1 – 2 THz, such as superconductor-insulator-superconductor (SIS) tunnel junctions and superconducting hot electron bolometers (HEBs)[7][8]. A number of photon detectors on the higher frequency side that are based on extrinsic semiconductors are a viable option for some applications. Extrinsic Ge: Ga photodetectors, for example, offer sensitivities in orders of magnitude better in direct mode

than superconducting bolometers operating at the same temperatures[9].

Despite the progress, the large-format array detectors required for practical imaging applications are still unavailable. It seems likely that evolutionary improvements and scaling of present technologies may not meet these requirements or could be prohibitively expensive, which would make alternative device concepts and materials worth considering.

Compound semiconductors, such as GaAs/AlGaAs, provide reliable and well-established material systems that can be used for making quantum-well photodetectors in a targeted spectral range. The devices are based on intersubband absorption in quantum wells (QWs) and a suitable band structure is achieved with an appropriate width for the QW layer and a suitable composition for the alloy in the barrier layers. These were primarily used for near- and middle-infrared devices

until recently. Their processing technology is fully mature and large-format infrared arrays with up to 1024×1024 pixels have been demonstrated^[10]. The optimal design for a QW photodetector with a minimal level of dark current corresponds to a situation where the first excited state in the quantum well is aligned with the top of the barrier (bound to a quasi-bound configuration). If we apply a similar methodology to the range between 1 – 8 THz, the parameters of the QW structure will correspond to low aluminum fractions of a few percent (1 – 5 %) and QW widths of 10 – 30 nm^[5].

A band diagram of a QW structure with an intersubband resonance frequency of 3 THz (wavelength: $\sim 100 \mu\text{m}$) is shown in Fig. 1. The structure contains 18 -nm GaAs QW and 80 -nm AlGaAs barriers with an Al alloy fraction of 2 %. To activate intersubband absorption, the centre of the well is doped with Si, which populates the QW's ground subband E_1 . The barriers are undoped. Detector samples have 20-repetitions of such QW sandwiched between $0.4 \mu\text{m}$ top and $0.8 \mu\text{m}$ bottom contact layers (Fig. 2).

We intend to select a doping concentration that ensures almost fully occupied E_1 . In the case of only one occupied subband and low operating temperatures such that $kT \ll E_2 - E_1$, we can write a simple formulae linking the Fermi level, E_F , and the two-dimensional density of electron gas in the well, n_w , as $n_w = (m^*/\pi \hbar^2)(E_F - E_1)$,

where m^* is the electron effective mass. The upper limit for the doping concentration, n_w^* , corresponds to a situation where E_F is situated just below the subband E_2 so that $n_w^* = (m^*/\pi \hbar^2)(E_2 - E_1) = (m^*/\pi \hbar^2)\Delta E_{21}$. In our detector, the gap between the subbands is $\Delta E_{21} = 11.1 \text{ meV}$, which corresponds to $n_w^* = (m^*/\pi \hbar^2)\Delta E_{21} \approx 3.1 \times 10^{11} \text{ cm}^{-2}$. The doping levels resulting in two-dimensional density higher than n_w^* would cause E_2 to be partially filled and create the possibility of an increased dark current and broadening of the spectral response of the photodetector without any improvements in photoabsorption characteristics at the targeted peak frequency. The actual value of n_w selected for our samples was about one third of n_w^* , which corresponds to a bulk density of $5.6 \times 10^{16} \text{ cm}^{-3}$.

Optimal doping of contact layers, n_c , should ensure stable low-resistivity ohmic contacts and at the same time sufficient transparency for frontside illumination of the detector. Because of the intended low operating temperature of the device (below 10 K) a relatively high doping level of $n_c = 2 \times 10^{18} \text{ cm}^{-3}$ has been selected. Transmittance measurements with terahertz time-domain spectroscopy (THz TDS) of 1 – 4 THz revealed that only a few percent of incoming radiation goes through the contact layer (Fig. 3). Transmittance improves to more than 60 % if the doping in the layer is decreased to $1 \times 10^{17} \text{ cm}^{-3}$; however, we have not yet tested the low-tem-

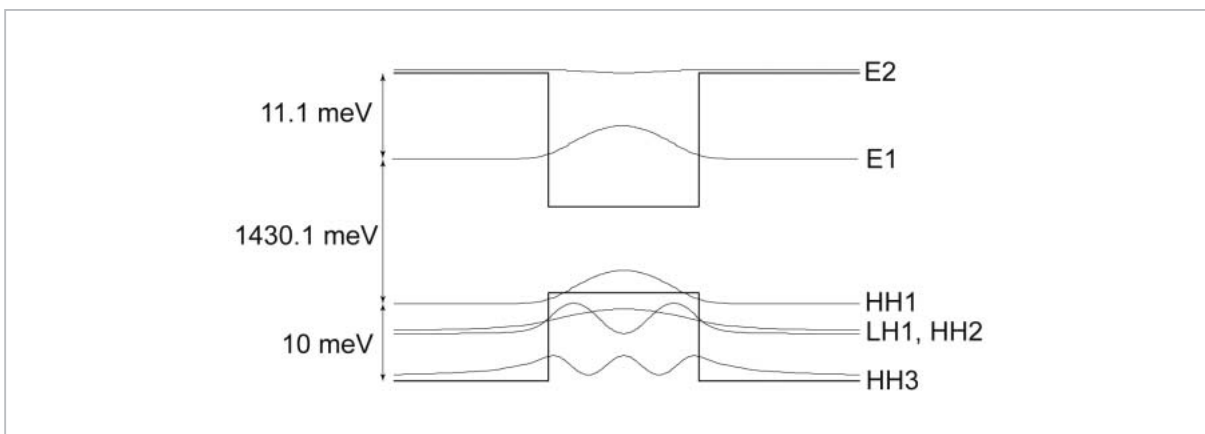


Fig. 1 Band diagram of the QW structure with an intersubband resonance frequency of 3 THz (wavelength $\sim 100 \mu\text{m}$). The structure consists of 18-nm GaAs QW and AlGaAs barriers with an Al alloy fraction of 2 %.

| | | |
|---|----------------------|--------|
| n ⁺ -GaAs (Si doped, $2 \times 10^{18} \text{ cm}^{-3}$) | top contact layer | 400 nm |
| Al _{0.02} Ga _{0.98} As | | 80 nm |
| GaAs (4-14 nm, Si doped, $1 \times 10^{17} \text{ cm}^{-3}$) | | 18 nm |
| Al _{0.02} Ga _{0.98} As | | 80 nm |
| GaAs (4-14 nm, Si doped, $1 \times 10^{17} \text{ cm}^{-3}$) | | 18 nm |
| | | • |
| | | • |
| | | • |
| GaAs (4-14 nm, Si doped, $1 \times 10^{17} \text{ cm}^{-3}$) | | 18 nm |
| Al _{0.02} Ga _{0.98} As | | 80 nm |
| GaAs (4-14 nm, Si doped, $1 \times 10^{17} \text{ cm}^{-3}$) | | 18 nm |
| Al _{0.02} Ga _{0.98} As | | 80 nm |
| n ⁺ -GaAs (Si doped, $2 \times 10^{18} \text{ cm}^{-3}$) | bottom contact layer | 800 nm |
| Semi-insulating GaAs substrate | | |

Fig.2 Schematic layout of MBE grown THz quantum well photodetector structure

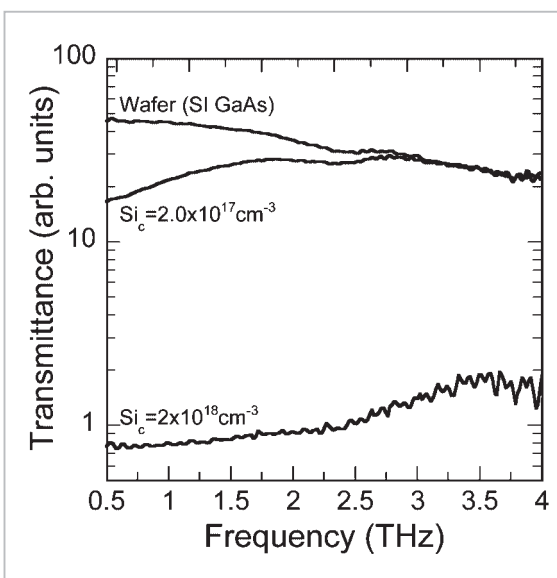


Fig.3 Effect of Si doping concentration on THz transmittance through the QW structure measured with time-domain spectroscopy (THz TDS). The contact layers doped to $2 \times 10^{18} \text{ cm}^{-3}$ transmit only a few percent of incoming radiation. Transmittance improves to up to 30 % if the concentration is decreased to $2 \times 10^{17} \text{ cm}^{-3}$

perature properties of contacts with a doping concentration lower than $1 \times 10^{18} \text{ cm}^{-3}$.

Another critical aspect of the detector's design is the selection of the barrier thickness that directly affects various tunneling mechanisms of dark current. The combined effects of different barrier widths and in-well doping concentrations on the expected dark current were numerically simulated, and a barrier width of 80 nm was selected as optimal for an

expected tunneling current density below 10^{-6} A/cm^2 .

Samples were grown by Molecular Beam Epitaxy (MBE) on semi-insulating GaAs substrates. X-ray diffraction, Scanning Electron Microscopy/Energy Dispersive Spectrometer (SEM/EDS), and Photoluminescence (PL) measurements were used to determine the composition, period, and energy-level structure of the samples. Despite the low Al content (2 %), we obtained consistent results with MBE growth and observed only minor deviations from the designed parameters.

The samples were processed into single-element square-shaped mesas of different sizes using standard processing techniques. To satisfy selection rules for intersubband absorption so that normally incident THz radiation can be absorbed by the structure, a one-dimensional metal grating coupler was patterned on the top surface of the mesas, which also served as the top electrode of the photodetector. Following conventional design considerations for the specific cutoff wavelength λ_c , samples with 100- μm (λ_c), 50- μm ($\lambda_c/2$) and 25- μm ($\lambda_c/4$) period gratings were fabricated [11]. The experimental results presented in this report were taken on a $1 \times 1 \text{ mm}^2$ photodetector with a 50- μm -period grating.

Detector samples were mounted in a mechanical cryocooler, which had the facility to stabilize the temperature in the range $T = 3 - 300 \text{ K}$. Dark current measurements were taken when the detector was completely surrounded by a cold shield, which was kept at the temperature $T = 40 \text{ K}$. In the case of photoelectric measurements, the samples were exposed to external photon flux through a filter module that was attached to the cold shield (and kept at the same temperature) and a room temperature Teflon window on the outer shield of the cryocooler with a resulting field of view of 60° . A filter module containing a set of filters served to block visible, near- and mid-infrared light and provide a well-defined band-pass within the targeted THz spectral range. The spectral response of the photodetector was measured using a Fourier Trans-

form Spectrometer (FTS).

Temperature dependence of the dark current versus applied electric field is shown in Fig. 4. The detector observed stable operation in the bias voltages between ± 60 mV and operating temperatures down to 3 K. Variation of the bias between negative and positive voltages did not produce hysteresis of the current-voltage characteristics, indicating a good contact property even at cryogenic temperatures. As expected, only two dark current mechanisms are present in the data. Thermionic emission related current with its exponential dependence on temperature dominates down to $T = 6$ K. At lower temperatures, the thermally assisted tunneling becomes the main mechanism of current flow. A more detailed view of a gradual transition from classical thermionic to quantum-mechanical tunneling is shown in Fig. 5. The curve flattens out at around $1 \mu\text{A}/\text{cm}^2$, with weak dependence on temperature. This indicates that other possible current mechanisms, such as resonance interwell and impurity assisted tunneling, are suppressed by 80 nm barriers to negligible levels. By fitting the standard model (e.g. [12]-[14]) of

the thermionic component of the dark current $J_D \sim T_{\text{exp}}(\Delta E_a/kT)$ to experimental data, activation energy $\Delta E_a = E_2 - E_F = 10.5$ meV was obtained, which gives the value of $E_F \sim 1$ meV. Estimation of E_F from the in-well doping concentration given by $E_F = \pi \hbar^2 n_w / m^* = 3.6$ meV indicates that an effective doping seems to be lower than a design value $n_w = 1 \times 10^{11} \text{ cm}^{-2}$.

The responsivity of the detector was measured using a calibrated blackbody source. Responsivity of 13 mA/W at an electric bias of 40 mV and an operating temperature of 3 K was obtained by comparing current-voltage characteristics under different photon flux conditions. A low responsivity value is a result of a significant loss of incoming radiation in the highly doped top contact layer and relatively inefficient coupling of a simple one-dimensional grating coupler used in the devices. As indicated earlier, by decreasing the doping concentration in the contact layer its transmission can be improved up to 60 %, which would directly enhance the responsivity. Further tests of such contacts are necessary to ensure good electrical properties at cryo-

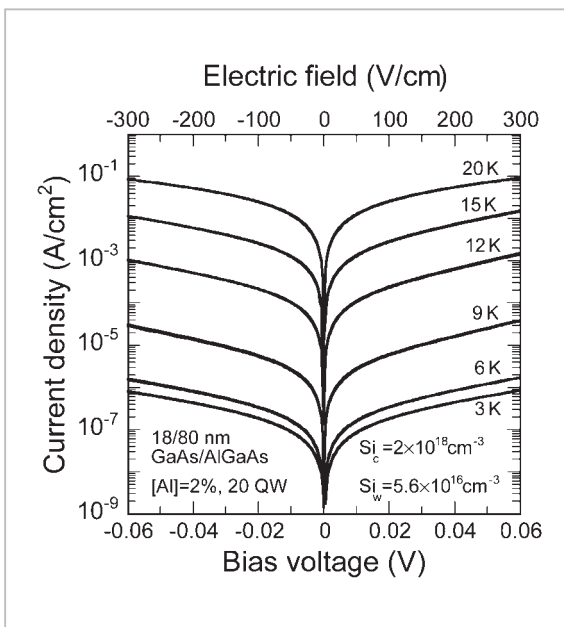


Fig.4 Bias and temperature dependence of dark current

The device observed stable operation between ± 60 mV with virtually symmetrical characteristics

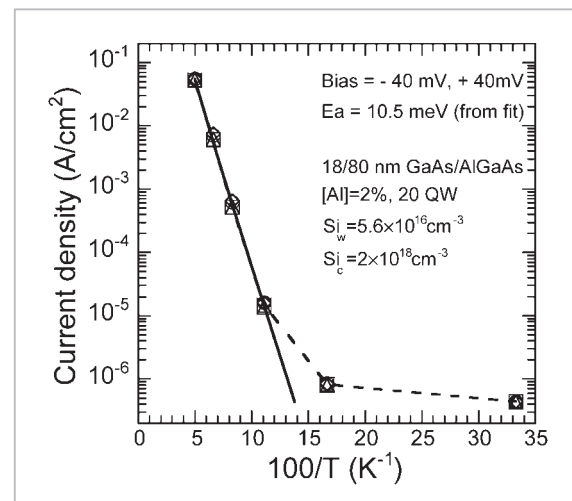


Fig.5 Temperature dependence of the dark current at ± 40 mV bias voltages

A solid line represents a fit by the standard model of the thermionic component $J_D \sim T_{\text{exp}}(\Delta E_a/kT)$ with $\Delta E_a = 10.5$ meV. Below 6K the current flattens out at around $1 \mu\text{A}/\text{cm}^2$ and is limited by thermally assisted tunneling through the barriers.

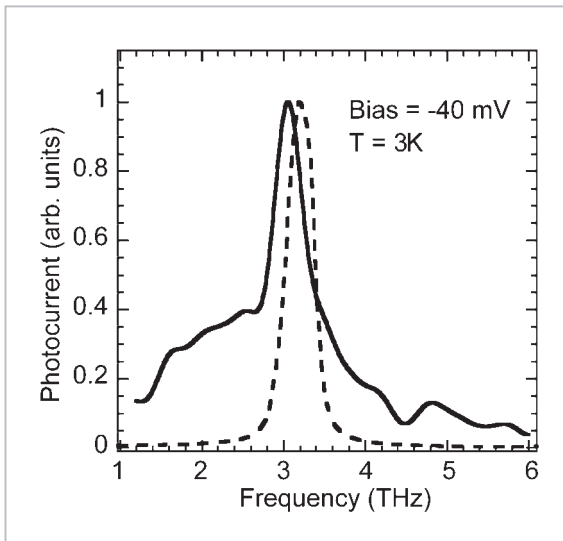


Fig.6 Normalized spectrum of detector's photoresponse (solid curve) compared with the results of numerical simulations

Observed response is close to the designed detection frequency. The model assumed a set of identical wells, a constant 2 % Al content in the barriers and a uniform electric field. Effect of bound-to-continuum transitions causing broadening of the spectrum were not considered in the calculations.

genic temperatures.

The spectral photoresponse of the detector is shown in Fig. 6. To improve a signal to noise ratio of the measurements, a battery powered feedback preamplifier with a built-in bias source was used. The positive bias of 40 mV is applied to the bottom contact while the top electrode is kept at virtual ground by the preamplifier's feedback. The measured peak frequency is in good agreement with the designed value; however, there is a discrepancy between the expected spectrum and the experiment, which can be explained by the limiting set of assumptions used in the model. For example, only a few eigen states from the continuum were included in the calculations, so the effect of bound-to-continuum transitions causing broadening of the spectrum could not be properly estimated. The model also assumed a set of identical wells, a constant 2 % Al content in the barriers and a uniform electric field. Because the resultant spectral response of the photodetector is an agree-

gate contribution of individual wells, any variations of the growth parameters and operating conditions in some of the wells may have an effect on the shape of the spectra. Asymmetry of the spectra with a more pronounced low frequency side is not yet understood. Among plausible mechanisms we can mention an effect of impurity-related absorption and non-uniform spectral characteristics of the diffractive coupler. Absorption in a doped QW can have a complex dependence on temperature, doping concentrations, and distribution of impurities within the well. Effects are related to a formation of a resonance impurity bands adjacent to QW subbands (e.g. $2p_z$ just below E_2) and an increase of a binding energy of the impurity (up to 2-3 times) compared to its three-dimensional bulk value[15]-[17]. At low temperatures and moderate doping levels, which are similar to our experimental conditions, the carrier freeze-out in a lowest impurity band can provide an alternative route for photon absorption in addition to the intersubband transitions[18][19].

Another effect, which can potentially alter the measured spectral response of the detector, involves the properties of the diffractive coupler. Dependence of the coupling efficiency on frequency can cause non-uniform coupling, which would mask the actual spectral characteristics of the detector. In future numerical simulations and experiments, we will try to clarify the underlying mechanisms explaining the result of experiments.

In conclusion, we have successfully demonstrated the operation of a THz frontside-illuminated GaAs/AlGaAs quantum well photodetector based on intersubband absorption in quantum wells (QWs) with a targeted peak frequency of 3 THz. Design considerations and results of the experiments indicate that significant improvement in performance can be attained by optimizing the in-well and contact doping concentrations and improving the design of the grating coupler.

References

- 1 R. Köhler, A. Treducucci, F. Beltram, H. E. Beere, E. H. Linfield, A. G. Davies, D. A. Richie, R. C. Iotti, and F. Rossi, "Terahertz semiconductor-heterostructure laser", *Nature* 417, 156, 2002.
- 2 B. S. Williams, S. Kumar, Q. Hu, and J. L. Reno, "Operation of terahertz quantum-cascade lasers at 164 K in pulsed mode and at 117 K in continuous-wave mode", *Opt. Express* 13, 3331, 2005.
- 3 L. Ajili, G. Scalari, N. Hoyler, M. Giovannini, and J. Faist, "InGaAs–AlInAs/InP terahertz quantum cascade laser", *Appl. Phys. Lett.* 87, 141107, 2005.
- 4 H. Yasuda, I. Hosako, S. Miyashita, and M. Patrashin, "Terahertz electroluminescence from GaSb/AlAs quantum cascade laser", *Electron. Lett.* 41, 1062, 2005.
- 5 H. C. Liu, C. Y. Song, A. J. Spring-Thorpe, and J. C. Cao, "Terahertz quantum-well photodetector", *Appl. Phys. Lett.* 84, 4068, 2004.
- 6 H. Luo, H. C. Liu, C. Y. Song, and Z. R. Wasilewski, "Background-limited quantum-well photodetector", *Appl. Phys. Lett.* 86, 231103, 2005.
- 7 B. D. Jackson, G. de Lange, T. Zijlstra, M. Kroug, J. W. Kooi, J. A. Stern, and T. M. Klapwijk, "Low-noise 0.8-0.96 and 0.96-1.12 THz superconductor-insulator-superconductor mixers for the Herschel space observatory", *IEEE Transactions On Microwave Theory And Techniques*, 54 (2), 547-558, 2006.
- 8 J. J. A. Baselmans, M. Hajenius, J. R. Gao, A. Baryshev, J. Kooi, T. M. Klapwijk, B. Voronov, P. de Korte, and G. Gol'tsman, "NbN hot electron bolometer mixers: Sensitivity, LO power, direct detection and stability", *IEEE Transactions On Applied Superconductivity*, 15 (2), 484-489, 2006.
- 9 M. Fujiwara, T. Hirao, M. Kawada, H. Shibai, S. Matsuura, H. Kaneda, M. Patrashin, and T. Nakagawa, "Development of a gallium-doped germanium far-infrared photoconductor direct hybrid two-dimensional array", *Appl. Opt.* 42 (12), 2166, 2003.
- 10 S. D. Gunapala, S. V. Bandara, J. K. Liu, C. J. Hill, S. B. Rafol, J. M. Mumolo, J. T. Trinh, M. Z. Tidrow, and P. D. LeVan, "1024 × 1024 pixel MWIR and LWIR QWIP focal plane arrays", *Proc. SPIE Int. Soc. Opt. Eng.* 5783, 789, 2005.
- 11 W. J. Li and B. D. McCombe, "Coupling efficiency of metallic gratings for excitation of intersubband transitions in quantum-well structures", *J. Appl. Phys.* 71 (2), 1038, 1992.
- 12 B. F. Levine, *J. Appl. Phys.* 74 (8), R1, 1993.
- 13 M. A. Kinch and A. Yariv, "Performance limitations of GaAs/AlGaAs infrared superlattices", *Appl. Phys. Lett.* 55 (20), 1093, 1989.
- 14 G. Sarusi, S. D. Gunapala, J. S. Park, and B. F. Levine, "Design and performance of very long-wavelength GaAs/Al_xGa_{1-x}As quantum-well infrared photodetectors", *J. Appl. Phys.* 76 (10), 6001, 1994.
- 15 G. Bastard, "Hydrogenic impurity states in a quantum well: A simple model", *Phys. Rev. B* 24 (8), 4714, 1981.
- 16 C. Priester, G. Allan, and M. Lannoo, "Resonant impurity states in quantum-well structures", *Phys. Rev. B* 29 (6), 3408, 1984.
- 17 M. Carras, V. Berger, X. Marcadet, and B. Vinter, "Experimental evidence of a Mott transition in highly doped two-dimensional confined structures", *Phys. Rev. B* 70, 233310, 2004.
- 18 D. Stehr, C. Metzner, M. Helm, T. Roch, and G. Srasser, "Resonant impurity bands in semiconductor superlattices", *Phys. Rev. Lett.* 95, 257401, 2005.
- 19 M. Helm, W. Hilber, and T. Fromherz, "Infrared superlattices: A probe of the miniband dispersion and the structure of the impurity band", *Phys. Rev. B* 48 (3), 1601, 1993.



Mikhail Patrashin, Ph.D.
*Expert Researcher, Advanced
Communications Technology Group,
New Generation Network Research
Center*
*Terahertz Frontside-Illuminated
Quantum-Well Photodetector*



HOSAKO Iwao, Ph.D.
*Research Manager, Advanced
Communications Technology Group,
New Generation Network Research
Center*
*Terahertz Semiconductor Devices and
Their Application to Measurement
Systems*